Supramolecular Chemistry
Publication details, including instructions for authors and subscription information:
http://www.informaworld.com/smpp/title~content=t713649759

Perylene Diimide Dyes Aggregates: Optical Properties and Packing Behavior in Solution and Solid State

Yong-Shan Ma[a]; Chen-Hui Wang[ab]; Ying-Jie Zhao[a]; Ying Yu[a]; Ci-Xiang Han[a]; Xin-Jian Qiu[a]; Zhiqiang Shi[a]
[a] Department of Chemistry, Shandong Normal University, Jinan, P. R. China [b] Shandong JiaoTong University, Jinan, P. R. China

To cite this Article Ma, Yong-Shan , Wang, Chen-Hui , Zhao, Ying-Jie , Yu, Ying , Han, Ci-Xiang , Qiu, Xin-Jian and Shi, Zhiqiang(2007) 'Perylene Diimide Dyes Aggregates: Optical Properties and Packing Behavior in Solution and Solid State', Supramolecular Chemistry, 19: 3, 141 — 149
To link to this Article: DOI: 10.1080/10610270600902324
URL: http://dx.doi.org/10.1080/10610270600902324

Supramolecular Chemistry, April–May 2007 Vol. 19 (3), pp. 141–149

Taylor & Francis
Taylor & Francis Group

Perylene Diimide Dyes Aggregates: Optical Properties and Packing Behavior in Solution and Solid State

YONG-SHAN MA[a], CHEN-HUI WANG[a,b], YING-JIE ZHAO[a], YING YU[a], CI-XIANG HAN[a], XIN-JIAN QIU[a] and ZHIQIANG SHI[a,*]

[a]*Department of Chemistry, Shandong Normal University, 88 Wenhuadonglu Road, Jinan 250014, P. R. China;* [b]*Shandong JiaoTong University, 5 Jiaoxiao Road, Jinan 250023, P. R. China*

(Received 15 May 2006; Accepted 21 June 2006)

An electron acceptor and a donor of perylene diimide dyes (4a, 4b) were synthesized in an effective way. And the π–π interactions between perylene diimide dyes were discussed in solution and in solid state. The existence of weak π–π interactions in 4a, 4b and their mixture was confirmed with UV/vis and fluorescence spectra in dilute solution. Furthermore, the ^{1}H-NMR studies displayed strong π–π interactions in concentrated solution. The packing behavior in solid state was discussed with solid state fluorescence, confocal fluorescence micrograph, scanning electron microscopy and powder X-ray diffraction, indicating stronger intermolecular interactions of 4a–4b than that of 4a–4a or 4b–4b.

Keywords: Perylene diimide; π–π Interactions; Self-assembly

INTRODUCTION

Non-covalent supramolecular interactions such as aggregation play a major role in controlling molecular organization in materials and an in depth knowledge of these interactions is fundamental for predicting their structure-property relationships [1–4]. With a planar π surface, the perylene-3,4,9,10-tetracarboxidiimide (PDI) has attracted recent interest in self-organization because it can be conveniently prepared and forms ordered structures [5–11]. In addition, as the significant n-type semiconductor, PDI possess brilliant colors, particularly promising optical properties, and outstanding chemical, thermal, and photochemical stability [12–15]. In the perylene tetracarboxylic diimide aggregation, the weak interactions directing the self-organization process come mainly from π–π molecular orbital overlaps [16]. Although the stacking of the planar π-systems of perylene diimide dyes is well documented in solution and in the crystal structures of the perylene pigments through UV/Vis, fluorescence studies and other calculation methods such as the Gibbs aggregation energies [17–22], the π–π interactions and packing behavior between two different perylene pigments haven't been discussed and the role of molecular packing in determining solid state fluorescence and structral characters of organic molecules is an area that is still not well understood. In this paper an electron donor of 1,7-Bis (N-pyrrolidinyl)-N,N′-dicyclohexyl perylene-3,4,9,10-tetracarboxylic diimide and an electron acceptor of 1,7-Bis(p-tert-butylphenoxy)-N,N′-Dicyclohexyl perylene-3,4,9,10-tetracarboxylic diimide were chosen as building blocks. Herein, we report the synthesis and packing behavior of two dyes in solution and solid states.

RESULTS AND DISCUSSION

Synthesis

For the preparation of soluble substituted perylene diimide dyes at the carbocyclic scaffold in the so-called bay-area (position 1, 6, 7, and 12), like compound **4**, one strategy proved to be successful. By this approach, the bromination of perylene bisanhydride **1** at the bay-area was carried out firstly. Then nucleophiles containing oxygen or nitrogen such as phenol or pyrrolidine were incorporated by nucleophilic displacement of bromine substituents to afford disubstituted derivative, which further was treated with corresponding

*Corresponding author. E-mail: zshi@sdnu.edu.cn

ISSN 1061-0278 print/ISSN 1029-0478 online © 2007 Taylor & Francis
DOI: 10.1080/10610270600902324

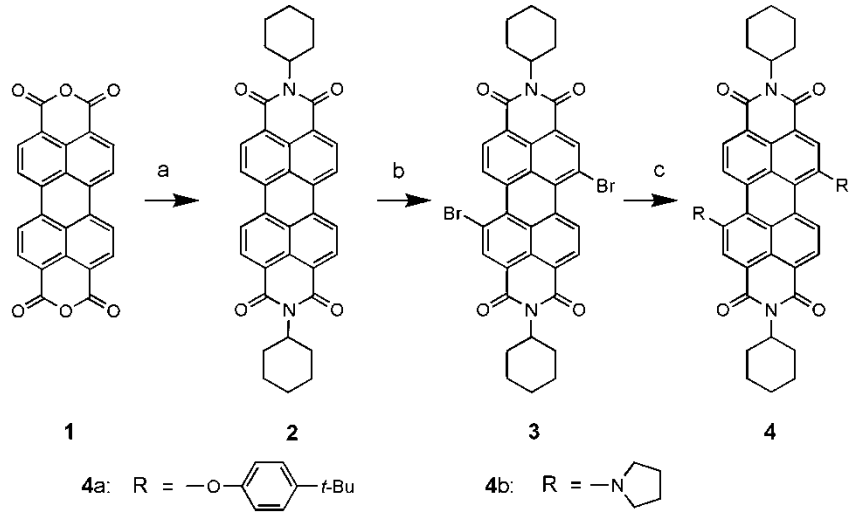

SCHEME 1

aromatic or aliphatic amine in solvent catalyzed with Lewis acid to yield the target compounds [9,10,23–25]. However, owing to the poor solubility, the significant dibromo product was obtained with unreasonable yield in bromination step. Usually containing excessive mono- and tribrominated byproducts, the resulting mixture obtained in bromination step was used directly in next step without isolation. Therefore, the isolation of disubstituted derivative from mono- and trisubstituted derivatives was even more difficult in next step.

By our strategy (Scheme 1), **1** was refluxed in cyclohexane firstly to give the diimide **2** with a yield of 100%. Compound **2** was bromated with bromine in dry dichloromethane to give 1,7-bromide **3** with a yield reaching to 93%. By a substitution reaction from **3** in N-methyl-2-pirrolidone (NMP) using potassium carbonate as base, the compound **4**a was prepared in a yield of 90%. Compound **4**b was synthesized according to a literature method [25]. This route was facile and efficient. Soluble diimide **2** was obtained in first step with neither catalyst nor isolation process. In the bromination step, no tribromo byproduct was yielded. And by controlling the concentration of bromine in reaction mixture and the reaction time, the monobromide product can be selectively obtained in good yield. For the synthesis of compound **4**a, much cheaper potassium carbonate was used as base instead of cesium carbonate formerly used.

π–π Interactions between Perylene Diimide Dyes 4a and 4b in Solution

For perylene diimide, the electronic absorption had a pronounced coupling to the vibronic features corresponding to $\upsilon = 0 \rightarrow \upsilon' = 0$, 1, 2 and 3 transitions, where υ and υ' were quantum vibrational numbers of the ground and excited states, respectively. As free monomer, normal progression of Franck-Condon factors were $A^{0\rightarrow0} > A^{0\rightarrow1} > A^{0\rightarrow2} > A^{0\rightarrow3}$. However, as the monomer begins to self-aggregate, the $0 \rightarrow 1$ and $0 \rightarrow 2$ transition increased [16,26]. Figure 1 showed the UV/vis absorption spectra of compound **4**a, **4**b and their 1:1 mixture, which were normalized to unity because we were interested in showing the peak shapes. Compared with two main peaks at 547 nm and 511 nm in chloroform (not shown), two main peaks of compound **4**a blue-shifted to 534 nm, 501 nm in tetrahydrofuran (THF) and 531 nm, 496 nm in cyclohexane, respectively. From 10^{-6} M to 10^{-5} M, the $0 \rightarrow 1$ transition absorption of **4**a increased relatively both in THF and cyclohexane, indicating stronger π–π interactions in higher concentration. This $0 \rightarrow 1$ transition absorption increase was more obvious in cyclohexane than in THF. Compound **4**b,

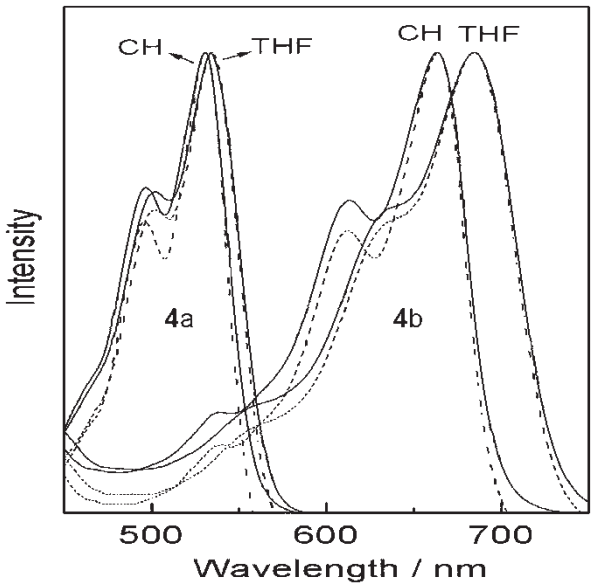

FIGURE 1 Normalized UV/vis absorption spectra in THF or cyclohexane (CH) for compound **4**a, **4**b (solid line: 10^{-5} M, dot line: 10^{-6} M).

a pyrrolidine substituted derivative, exhibited a good solubility in organic solvent and even in a polar solvent of ethanol. As a polar molecule, **4**b displayed obvious solvent effect in the absorption spectra. The main absorption peak of **4**b blue-shifted from 699 nm in chloroform (not shown) to 684 nm in THF and 663 nm in cyclohexane, respectively. The concentration (10^{-6} M $\sim$ 10^{-5} M) dependent $0 \rightarrow 1$ transition absorption relative intensity increased more in cyclohexane than that in THF, suggesting strengthened $\pi-\pi$ interactions between **4**a and **4**b took place both in THF and in cyclohexane at 10^{-5} M scale.

The fluorescence spectra of the 10^{-4} M 1:1 mixture of **4**a and **4**b in chloroform and the references of 10^{-4} M **4**a and 10^{-4} M **4**b were recorded excited at 576 nm and 737 nm, respectively (Fig. 2). Excited at 576 nm, the fluorescence spectrum revealed pronounced changes compared with **4**a. i) The emission intensity of the mixture at 585 nm was quenched by a factor of 5.2; ii) the maximum of the mixture blue-shifted 2 nm; iii) a broad weak peak at emission extent of **4**b was observed. Excited at 737 nm, the emission peak of the mixture blue-shifted 2 nm and the intensity increased weakly compared with **4**b owing to the additional contribution of **4**a in this area. All of the changes could be interpreted as stronger $\pi-\pi$ interactions between **4**a and **4**b (**4**a–**4**b). As an N atom substituted derivatives, **4**b was a comparative electron donor in comparison with **4**a. The additional electron donor–accepter interaction strengthened the **4**a–**4**b $\pi-\pi$ interactions, resulting in a dominant cofacial $\pi-\pi$ stacking between **4**a and **4**b. Correspondingly, the **4**a–**4**a and **4**b–**4**b $\pi-\pi$ stacking played a less important role in the mixture. Therefore, both of the emission peaks of **4**a and **4**b in the mixture blue-shifted 2 nm owing to the intermolecular interactions between **4**a and **4**b. The strong quench of emission at 585 nm and the increase of emission at 749 nm were mainly due to the $\pi-\pi$ molecular orbital overlaps between **4**a and **4**b, which resulted in the energy transfer. In addition, the strengthened $\pi-\pi$ aggregation in the mixture led to a stronger aggregation of the mixture in solution, which decreased the intensity of all emission of the mixture.

Further insight into the $\pi-\pi$ interactions in more concentrated solution was gained by ^{1}H-NMR study. In general, the self-aggregation depended on the solubility, i.e. the $\pi-\pi$ stacking was favored in poor solvent. In good solvent such as chloroform, perylene derivatives existed predominately as free monomers at dilute concentration. Only when the initial concentration was high enough (>1 mM), self-aggregation began to take shape. As shown in Fig. 3, aromatic hydrogen of perylene parent at 5 (γ), 6 (β), 8 (α) positions of both **4**a and **4**b yielded obvious upfield shift as the concentration increased from 5×10^{-3} M (C_1) to 10^{-2} M (C_2) in $CDCl_3$. Those results were in good agreement with previous research [16]. When magnetic field was applied, all of the aromatic planes of parent perylene diimides aligned in a perpendicular direction to outer magnetic field. In a J-tape [17,26,27] aggregation, all of α, β and γ-Hs for **4**a or **4**b were located in an antimagnetic region of a neighbor perylene diimide aromatic plane as well as in a paramagnetic region of another neighbor perylene diimide aromatic plane. But the antimagnetic interaction was centralized in aromatic loop, while the paramagnetic interaction was decentralized out of the aromatic plane. Therefore the net effect was antimagnetic in the case of **4**a or **4**b $\pi-\pi$ stacking. Thus, the concentration dependent $\pi-\pi$ stacking led to a upfield shift in this case. In the mixture **4**a–**4**b, however, downshift of α, β and γ-Hs of both **4**a and **4**b was observed upon the mixture concentration increasing from 5×10^{-3} M to 10^{-2} M. Owing to stronger $\pi-\pi$ interactions between **4**a and **4**b, an alignment of

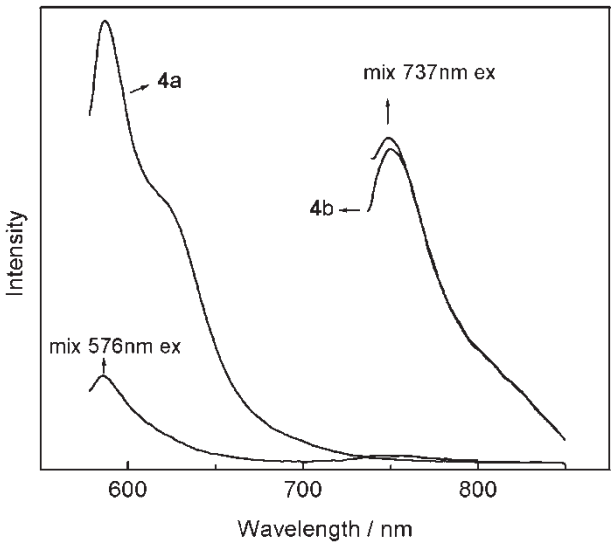

FIGURE 2 Emission spectra of 10^{-4} M **4**a, **4**b and the 1:1 mixture of **4**a–**4**b in chloroform. The excitation wavelength was 576 nm for **4**a, 737 nm for **4**b and both for the mixture.

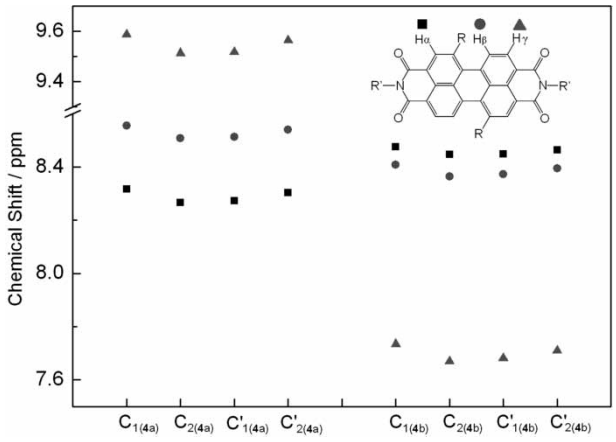

FIGURE 3 Observed chemical shifts for Hα, Hβ and Hγ of **4**a, **4**b and **4**a–**4**b mixture. C_1: 5×10^{-3} M, C_2: 10^{-2} M, C': mixture of **4**a–**4**b.

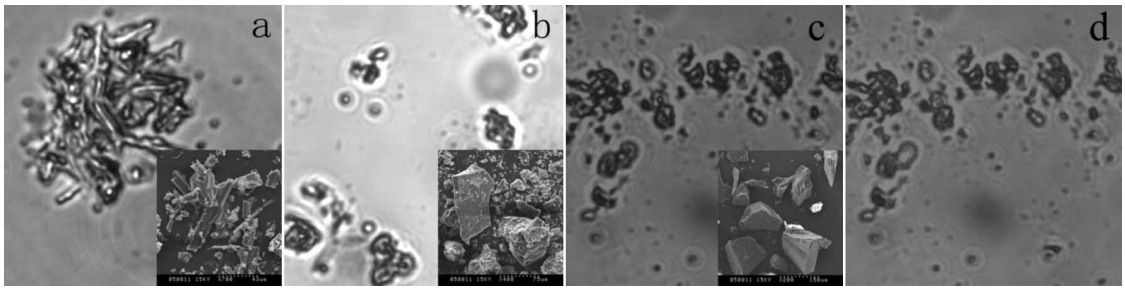

FIGURE 4 200 μm × 200 μm confocal fluorescence micrograph of mesoscopic superstructures for (a) **4**a excitation at 590 nm, (b) **4**b excitation at 720 nm, (c) **4**a–**4**b mixture excitation at 590 nm, (d) **4**a–**4**b mixture of the same field excitation at 720 nm. Excitation 40μW, fluorescence intensity 100–1500 counts per pixel. Insert: SEM images of corresponding samples.

4a–**4**b–**4**a–**4**b was favorable in the mixture. The π–π molecular orbital overlaps between **4**a and **4**b together with the electron donor–acceptor interaction resulted in a delocalizing of PDI parent electrons in the mixture. The electron delocalization decreased the antimagnetic interaction affected by the aromatic hydrogen, while the total paramagnetic interaction affected changed little. Accordingly, the aggregation of the mixture led to all of the aromatic hydrogen protons at parent perylene in the mixture downshift.

Structural Characterization of the Samples in Solid State

Laser scanning confocal microscopy (LSCM) excluded out-of-focus information by focusing through a small aperture (a confocal pinhole). This feature ensured that information in the image arrived only from a particular depth of the specimen, hence providing a method to observe an optically sliced section of the object in a sample. The optical sections thus obtained could be reconstructed into a three-dimensional (3D) image by an image processing. Therefore, LSCM was an excellent tool for studying the phase-separated structures of a fluorescent mixture. As shown in Fig. 4, the particles observed for different samples were similar to corresponding SEM images both in morphologies and in sizes. As for sample **4**a, the morphology was rod-like. Owing to the lower resolution of the confocal microscope about 200 nm the fine morphologies could not be distinguished as in the SEM. However, some variations on the fluorescence intensity were noted. With a higher fluorescence efficiency excited at 590 nm, The fluorescence of the **4**a–**4**b mixture sample was brighter than that excited at 720 nm in the same field. Therefore, Fig. 4c looked clearer than Fig. 4d. Those results indicated that no isolated phase of **4**a or **4**b appeared under LSCM observation.

The surface morphologies of the solids of **4**a, **4**b and **4**a–**4**b mixture were investigated by SEM. As could be seen from Fig. 5a, besides some small fragments resulted from ultrasonic treatment the cubic structure with glossy surface was predominant for **4**a. This cuboid was constructed with uniform thinner layer cubic structures with a constant thickness of 700 nm. Similar to **4**a, **4**b also comprised layer structure (Fig. 5b). But the layer was coarse and looked like lots of crimples on the surface. The observable thinnest layer was about 100 nm in thickness, which assembled to a thicker layer of about 5 μm. Compared to **4**b, the mica-like layer structure was clear for 1:1 mixture of **4**a–**4**b. Each layer was about 2 μm in thickness, and was made up of thinner layers. In general, **4**a, **4**b and **4**a–**4**b mixture were similar in layer structure, but they had different fine microstructures.

The molecular order within the congeries of **4**a, **4**b and **4**a–**4**b mixture was determined by X-ray diffraction. The X-ray diffraction trace from **4**a, **4**b and **4**a–**4**b mixture were showed in Fig. 6. For **4**a, four strong well-resolved reflections were seen with 2θ value of 6.5°, 6.8°, 14.5°, and 19.1°. The crystalline peaks resulted from perylene diimides aggregation. The XRD

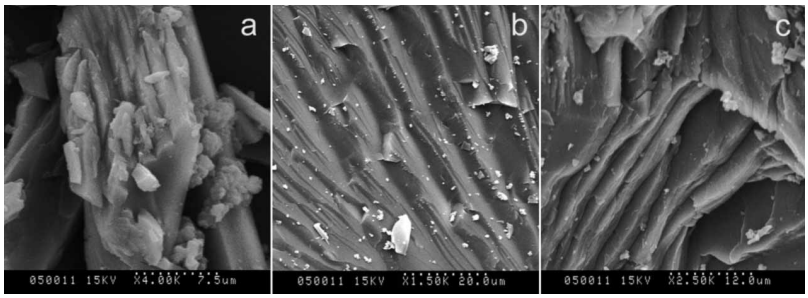

FIGURE 5 Cross-sectional SEM images of sample **4**a (a), **4**b (b) and **4**a–**4**b mixture (c).

patterns of **4**b and 1:1 **4**a–**4**b mixture showed two broad bands centered at $2\theta = 6.8°$ and 19.1°, which was consistent with the amorphous aggregation structures of **4**b and the mixture. However, the XRD pattern of 1.1:1 **4**a–**4**b mixture showed similar peaks as **4**a. This result revealed that the excess 10% **4**a self-aggregated to form crystalline, indicating that the aggregation of the mixture is almost 1:1.

The shapes of the fluorescence spectra of the samples **4**a, **4**b and **4**a–**4**b mixture in solid state (Fig. 7) were quite different from those fine distinct vibronic structure of PDI core in solutions. In the solid state, no distinguishable shoulder peak for fluorescence maximum of both **4**a and **4**b was observed, suggesting the presence of pronounced intermolecular interactions. The fluorescence spectra underwent a significant red shift in solid state (679 nm for **4**a and 821 nm for **4**b) compared to their chloroform solution (587 nm for **4**a and 750 nm for **4**b) despite the corresponding effective excitation wavelength blue shifted about 26 nm and 27 nm, respectively. **4**a and **4**b showed Stokes' shift values of 10 nm and 13 nm, respectively in chloroform solution, while the Stokes' shift values in their solid state were 129 nm and 110 nm, respectively. The marked red shift in their solid-state fluorescence spectra could therefore be clearly attributed to changes in molecular stacking of **4**a and **4**b. The red shift in the fluorescence spectra was also an indicative of the formation of aggregates [28,29]. Whereas, the blue shift of effective excitation wavelength in solid state could be generally attributed to the effective absorption transition from ground state to higher excited state.

Reference with pure **4**a and **4**b, a small blue shift of the fluorescence of the mixture was observed in solid state, which was similar to those in solution. An obvious shoulder peak over 800 nm was also observed when the **4**a–**4**b mixture was excited at 550 nm. These were presumed that a facile exciton migration or energy transfer occurred in the solid state from **4**a to **4**b owing to the close π–π stacking between **4**a and **4**b.

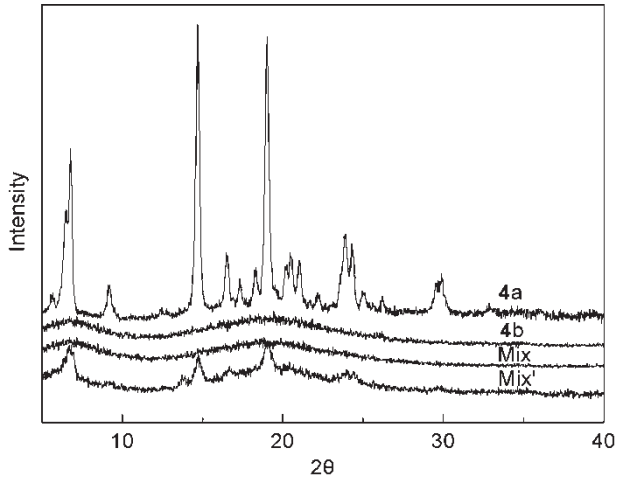

FIGURE 6 X-ray diffraction patterns of samples of **4**a, **4**b, 1:1 **4**a–**4**b mixture (Mix) and 1.1:1 **4**a–**4**b mixture (Mix').

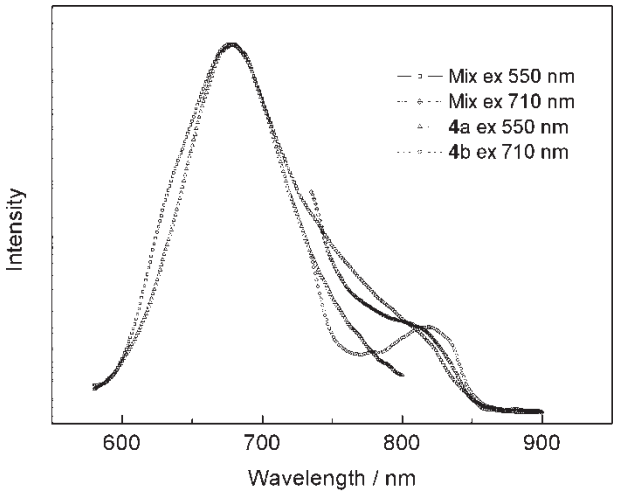

FIGURE 7 Solid-state fluorescence spectra of the powder samples of **4**a, **4**b and **4**a–**4**b mixture films (1 μm in thickness).

B3LYP/6-31G* Calculations

The packing behavior of **4**a, **4**b and **4**a–**4**b mixture could be partially interpreted by energies and geometries calculations performed with Gaussian 03 installed on a Windows PC. The geometries of the **4**a and **4**b were optimized with unrestricted DFT, incorporating the B3LYP functional and 6-31G basis set. The MO analysis of **4**a and **4**b showed that the highest occupied MO (HOMO) and lowest unoccupied MO (LUMO) were localized well in the perylene core (Fig. 8). Therefore, it seemed reasonable to assume that the interactions between the perylene cores played an important role in the packing behavior of **4**a and **4**b. The calculated HOMO, LUMO values were −0.20512 a.u., −0.11180 a.u. for **4**a and −0.18648 a.u., −0.11173 a.u. for **4**b respectively. HOMO-LUMO gaps were corresponding to λ_{max} of 524.4 nm (**4**a) and 611.2 nm (**4**b). This result agreed well with the experimental data (531 nm for **4**a and 663 nm for **4**b in cyclohexane). DFT calculations suggested that the phase of the **4**b HOMO matched the phase of **4**a LUMO, allowing donor–acceptor interactions.

The ground-state geometries calculated at B3LYP/6-31G* level had a core twist angle of the perylene core, i.e. the approximate dihedral angle between the two naphthalene subunits attached to the central benzene ring, which was 4.7° for the **4**a and 31.4° for **4**b (Fig. 9). With a torsional angle of less than 5°, the almost planar **4**a crystalized readily. However, more than 30° distortion from planarity imposed considerable constraints in the packing of **4**b in the solid state as well as in molecular aggregates, resulting in destabilization of the

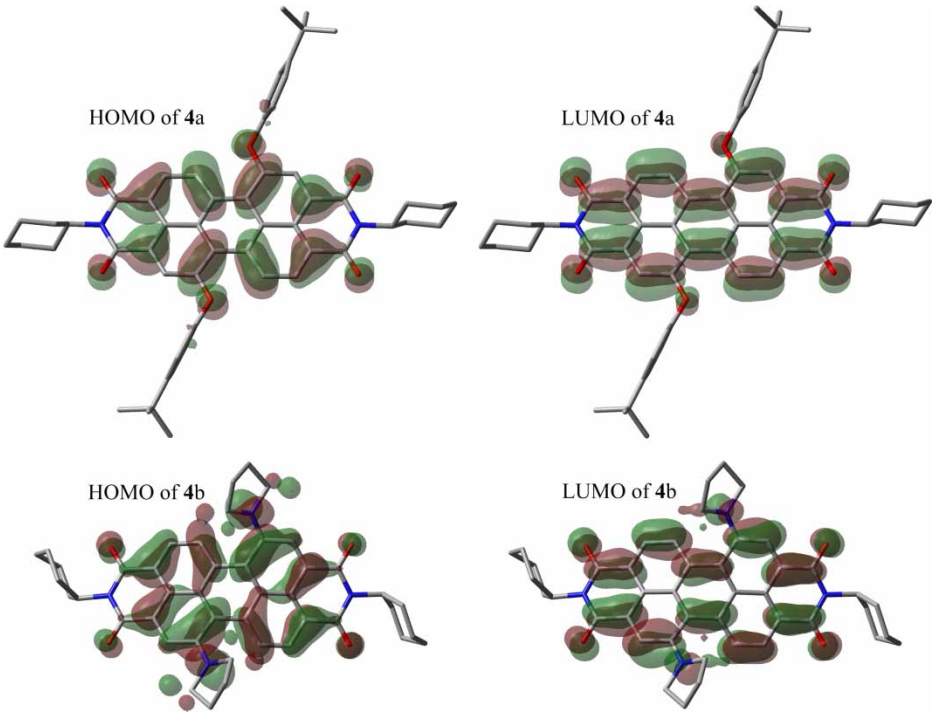

FIGURE 8 HOMO (left) and LUMO (right) of ground-state **4**a (above) and **4**b (below) at B3LYP/6-31G* level. Hydrogen atoms are not shown in the representation.

possible crystal structure. The advantage of this distortion was that it afforded much better soluble dyes. Accordingly, the solubility of **4**b increased remarkably. With stronger interactions between **4**a and **4**b than **4**a–**4**a or **4**b–**4**b, the significant out-of-plane twisted molecular structure of **4**b prevented crystallization of the **4**a–**4**b mixture.

CONCLUSION

In summary, we have described an effective pathway for the synthesis of two perylene diimide dyes of **4**a and **4**b. The packing behavior of **4**a, **4**b and their mixture were investigated with photophysical spectra in solution and structural characterization in solid state. The additional electron donor–acceptor interactions afforded a strengthened π–π stacking interactions between **4**a and **4**b.

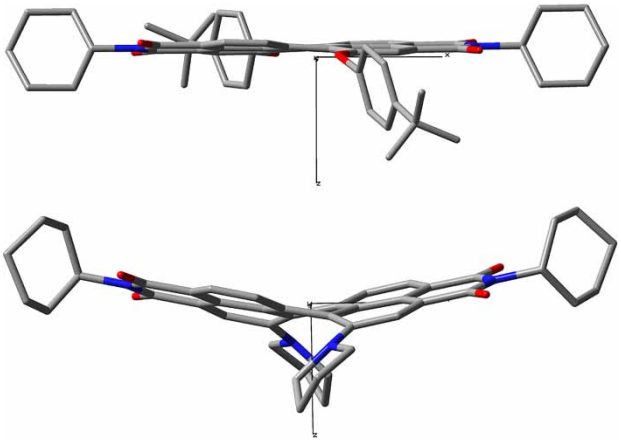

FIGURE 9 DFT (B3LYP/6-31G*) geometry-optimized structures of **4**a (above) and **4**b (below) shown with view along the short (y) axis. For the purposes of the simplified representation, hydrogen atoms are not shown.

EXPERIMENTAL

XRD patterns were recorded using a powder diffractometer (Philips PW1830) operating in the reflection mode with CuKα radiation and equipped with a grahite back momochromator. Solid state fluorescence spectra were recorded using the front face emission scan mode on a FLS920 fluorescence specroscopy. The laser scanning confocal microscopy observations were performed using an LSM410 with a 100 × objective or 60 × objectives at room temperature. Scanning electron microscopy measurements were carried out on a Hitachi S-570 instrument.

Synthesis

N,N′-Dicyclohexyl perylene-3,4,9,10-tetracarboxylic diimide (2)

In a 50 mL single-necked flask, 2.0 g perylene-3,4,9,10-tetracarboxylic dianhydride (5.1 mmol) and 30 mL cyclohexylamine were added. The mixture was refluxed for 24 h. The solvent was removed on the rotary evaporator to afford a red product (100%). ^{1}H-NMR (300 MHz, $CDCl_3$, ppm) δ 8.63 (d, 4H,

$J = 8.1$ Hz), 8.59 (d, 4H, $J = 8.1$ Hz), 5.06 (m, 2H), 2.60 (m, 4H), 1.90 (m, 4H), 1.78 (m, 6H), 1.40 (m, 6H); MS (Maldi-TOF): 554.27 (M^+); Anal. Calcd for $C_{36}H_{30}N_2O_4$: C, 77.96; H, 5.45; N, 5.05. Found: C, 77.85; H, 5.56; N, 5.34.

1,7-Dibromo-N,N′-dicyclohexyl perylene-3,4,9,10-tetracarboxylic diimide (3)

1.0 g compound **2** (1.8 mmol) was suspended in 10 mL dried dichloromethane, then 3 mL bromine diluted with 10 mL dried dichloromethane was dropped in under stirring for 10 min. The mixture was refluxed for 2 days. Excess bromine and solvent was removed. The residue was column chromatographed on silica with chloroform to afford a red product (93%). ^{1}H-NMR (300 MHz, $CDCl_3$, ppm) δ 9.45 (d, 2H, $J = 8.2$ Hz), 8.86 (s, 2H), 8.65 (d, 2H, $J = 8.2$ Hz), 5.01 (m, 2H), 2.53 (m, 4H), 1.92 (m, 4H), 1.75 (m, 6H), 1.44 (m, 6H); ^{13}C-NMR (75 MHz, $CDCl_3$, ppm, Appendix A, Figs. A2 and A4) δ 163.18, 162.62, 137.96, 137.83, 132.56, 132.46, 130.82, 129.84, 129.68, 129.06, 128.30, 127.94, 126.90, 123.65, 123.22, 120.64, 54.26, 29.07, 26.49, 25.37; MS (Maldi-TOF): 712.44 (M^+).

1,7-Bis(p-tert-butylphenoxy)-N,N′-dicyclohexyl perylene-3,4,9,10-tetracarboxylic diimide (4a)

1.07 g compound **3** (1.5 mmol), 0.54 g p-tert-butylphenoxy (3.6 mmol), and 0.69 g K_2CO_3 (5.0 mmol) were stirred in 15 mL NMP under argon at 120°C for 24 h. After being cooled to room temperature, the reaction mixture was poured into 50 mL water. The precipitate was filtered, repeatedly washed with water, and dried in a vacuum at 70°C. The product was column chromatographed on silica with chloroform to afford a red product (90%). ^{1}H-NMR (300 MHz, $CDCl_3$, ppm, Appendix A, Fig. A1) δ 9.54 (d, 2H, $J = 8.3$ Hz), 8.53 (d, 2H, $J = 8.3$ Hz), 8.29 (s, 2H), 7.48 (d, 4H, $J = 8.2$ Hz), 7.10 (d, 4H, $J = 8.2$ Hz), 5.01 (m, 2H), 2.53 (m, 2H), 1.89 (m, 4H), 1.75 (m, 2H), 1.40 (s, 18H), 1.28 (m, 12H); ^{13}C-NMR (75 MHz, $CDCl_3$, ppm) δ 163.67, 163.30, 155.36, 152.53, 148.10, 133.15, 129.94, 128.96, 128.61, 127.41, 124.88, 124.15, 123.54, 122.55, 119.23, 54.02, 34.53, 31.46, 29.68, 29.10, 26.52; MS (Maldi-TOF): 850.35 (M^+).

1,7-Bis(N-pyrrolidinyl)-N,N′-dicyclohexyl perylene-3,4,9,10-tetracarboxylic diimide (4b)

1.07 g compound **3** (1.5 mmol) was dissolved in 10 mL pyrrolidine, then 0.69 g K_2CO_3 (5.0 mmol) was added. The solution was heated with stirring at 50°C under dry nitrogen for 24 h. Excess pyrrolidine was removed and the residue was column chromatographed on silica with chloroform to afford a green product (95%). ^{1}H-NMR (300 MHz, $CDCl_3$, ppm, Appendix A, Fig. A3) δ 8.47 (s, 2H), 8.36 (d, 2H, $J = 7.9$ Hz), 7.66 (d, 2H, $J = 7.9$ Hz), 5.06 (m, 2H), 3.73 (m, 4H), 2.94 (m, 4H), 2.79 (m, 4H), 1.94 (m, 12H), 1.76 (m, 6H), 1.50–1.22(m, 6H); ^{13}C-NMR (75 MHz, $CDCl_3$, ppm; Appendix A, Figure A4) δ 164.62, 164.55, 149.98, 146.56, 135.50, 134.21, 130.01, 126.66, 123.86, 123.29, 122.37, 120.73, 119.68, 118.17, 53.73, 52.11, 29.67, 29.18, 26.62, 25.79, 25.60, 25.54; MS (Maldi-TOF): 692.48 (M^+).

The powder of 1:1 **4**a–**4**b mixture was obtained by evaporation of chloroform solvent from corresponding solutions at room temperature and then dryness in vacuum.

Acknowledgements

This work was supported by the National Natural Science Foundation of China (20473050 and 20531060).

References

[1] Gan, H.; Liu, H.; Li, Y.; Zhao, Q.; Li, Y.; Wang, S.; Jiu, T.; Wang, N.; He, X.; Yu, D.; Zhu, D. *J. Am. Chem. Soc.* **2005**, *127*, 12452.
[2] Liu, Y.; Li, Y.; Jiang, L.; Gan, H.; Liu, H.; Li, Y.; Zhuang, J.; Lu, F.; Zhu, D. *J. Org. Chem.* **2004**, *69*, 9049.
[3] Packer, M. J.; Dauncey, M. P.; Hunter, C. A. *J. Mol. Biol.* **2000**, *295*, 85.
[4] Yu, Y.; Wu, J.; Ma, Y.; Wang, C.; Shi, Z. *New J. Chem.* **2006**, *1*, 18.
[5] Li, Y.; Wang, N.; Gan, H.; Liu, H.; Li, H.; Li, Y.; He, X.; Huang, C.; Cui, S.; Wang, S.; Zhu, D. *J. Org. Chem.* **2005**, *70*, 9686.
[6] You, C.; Würthner, F. *J. Am. Chem. Soc.* **2003**, *125*, 9716.
[7] Neuteboom, E. E.; Meskers, S. C. J.; Meijer, E. W.; Janssen, R. A. *J. Macromol. Chem. Phys.* **2004**, *205*, 217.
[8] Sautter, A.; Kaletas, B.; Schmid, D. G.; Dobrawa, R.; Zimine, M.; Jung, G.; van Stokkum, I. H. M.; Cola, L. D.; Williams, R. M.; Würthner, F. *J. Am. Chem. Soc.* **2005**, *127*, 6719.
[9] Giaimo, J. M.; Gusev, A. V.; Wasielewski, M. R. *J. Am. Chem. Soc.* **2002**, *124*, 8530.
[10] Sinks, L. E.; Rybtchinski, B.; Iimura, M.; Jones, B. A.; Goshe, A. J.; Zuo, X.; Tiede, D. M.; Li, X.; Wasielewski, M. R. *Chem. Mater.* **2005**, *17*, 6295.
[11] van der Boom, T.; Hayes, R. T.; Zhao, Y.; Bushard, P. J.; Weiss, E. A.; Wasielewski, M. R. *J. Am. Chem. Soc.* **2002**, *124*, 9582.
[12] Lee, S. K.; Zu, Y.; Herrmann, A.; Geerts, Y.; Müllen, K.; Bard, A. J. *J. Am. Chem. Soc.* **1999**, *121*, 3513.
[13] Quante, H.; Geerts, Y.; Müllen, K. *Chem. Mater.* **1997**, *9*, 495.
[14] Law, K. Y. *Chem. Rev.* **1993**, *93*, 449.
[15] Kazmaier, P. M.; Hoffmann, R. *J. Am. Chem. Soc.* **1994**, *116*, 9684.
[16] Wang, W.; Han, J.; Wang, L.; Li, L.; Shaw, W.; Li, A. D. Q. *Nano Lett.* **2003**, *4*, 455.
[17] Würthner, F.; Thalacker, C.; Diele, S.; Tschierske, C. *Chem. Eur. J.* **2001**, *7*, 2245.
[18] Graser, F.; Hädicke, E. *Liebigs Ann. Chem.* **1980**, 1994.
[19] Graser, F.; Hädicke, E. *Liebigs Ann. Chem.* **1984**, 483.
[20] Hädicke, E.; Graser, F. *Acta Crystallogr.* **1986**, *42*, 195.
[21] Klebe, G.; Graser, F.; Hädicke, E.; Berndt, J. *Acta Crystallogr.* **1989**, *45*, 69.
[22] Zugenmaier, P.; Duff, J.; Bluhm, T. L. *Cryst. Res. Technol.* **2000**, *35*, 1095.
[23] Zinsou, A.; Veber, M.; Strzelecka, H.; Jallabert, C.; Fourre, P. *New J. Chem.* **1993**, *17*, 309.
[24] Percec, V.; Ahn, C. H.; Bera, T. K.; Ungar, G.; Yeardley, D. J. P. *Chem. Eur. J.* **1999**, *5*, 1070.
[25] Zhao, Y.; Wasielewski, M. R. *Tetrahedron Lett.* **1999**, *40*, 7047.
[26] Langhals, H.; Ismael, R. *Eur. J. Org. Chem.* **1998**, 1915.
[27] Beckers, E.; Meskers, S.; Schenning, A.; Chen, Z.; Wuerthner, F.; Marsal, P.; Beljonne, D.; Cornil, J.; Janssen, R. *J. Am. Chem. Soc.* **2006**, *128*, 649.
[28] Hädicke, E.; Graser, F. *Acta Crystallogr.* **1986**, *42*, 189.
[29] Duff, J. M.; Har, A. M.; Loutfy, R. O.; Eleryk, A. R. M. *Chem. Funct. Dyes* **1992**, *2*, 564.

APPENDIX A

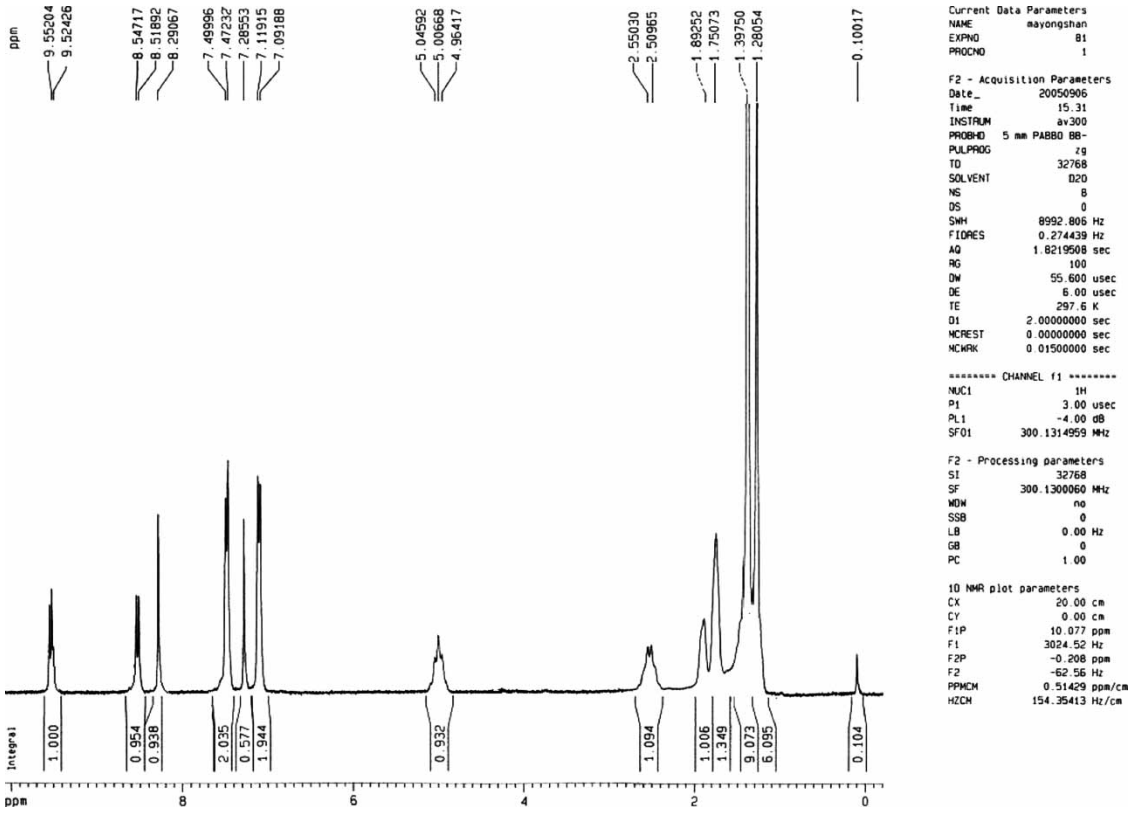

FIGURE A1 ^{1}H-NMR spectrum of compound **4**a.

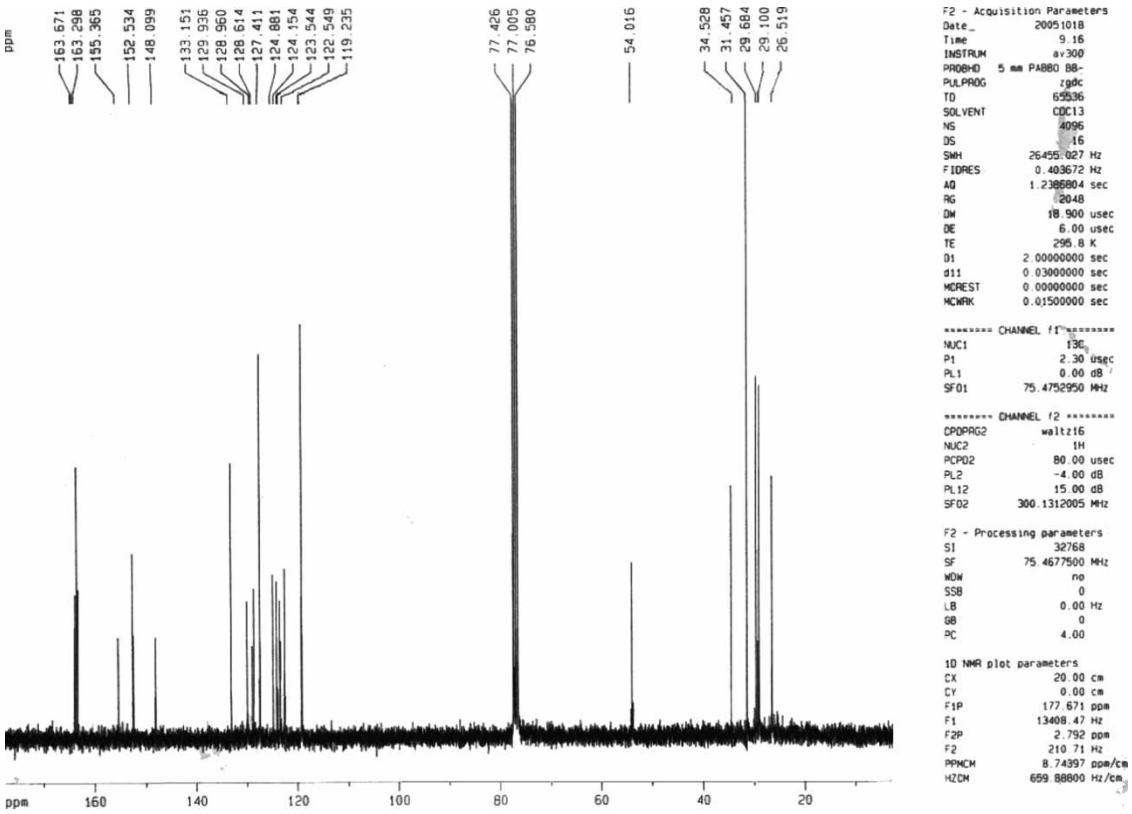

FIGURE A2 ^{13}C-NMR spectrum of compound **4**a.

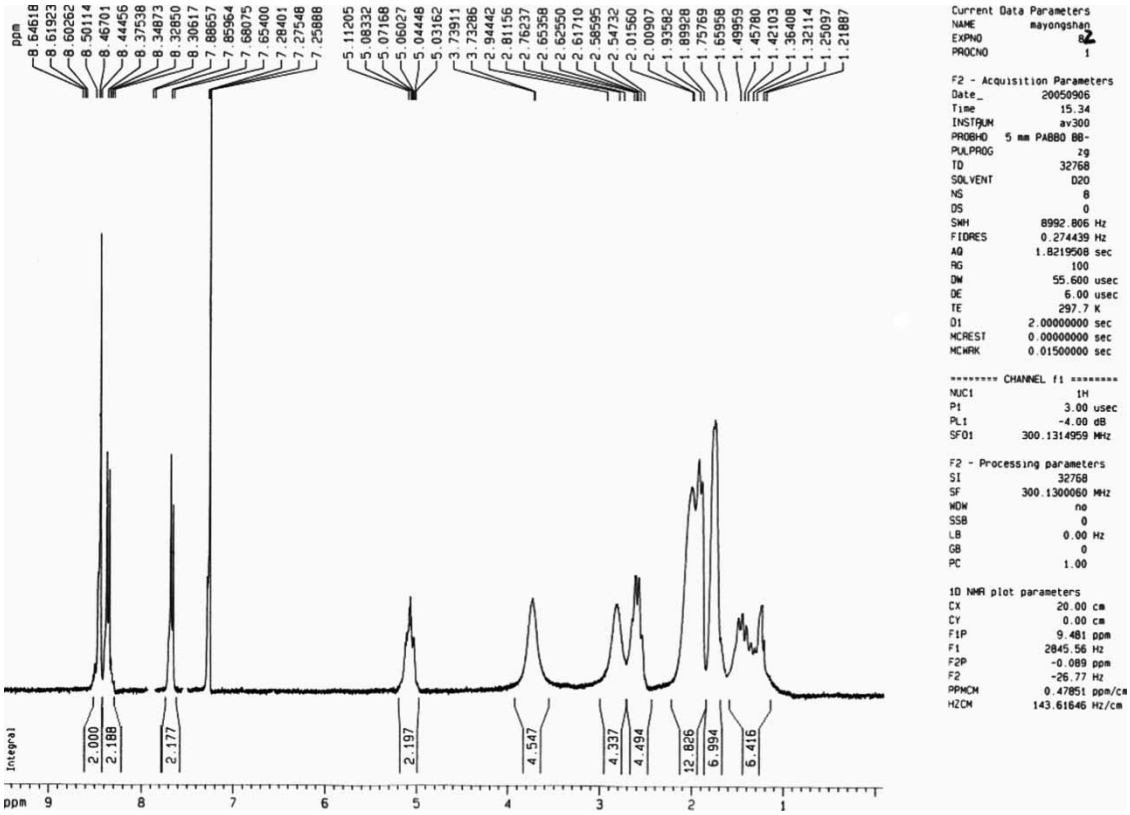

FIGURE A3 ^{1}H-NMR spectrum of compound **4**b.

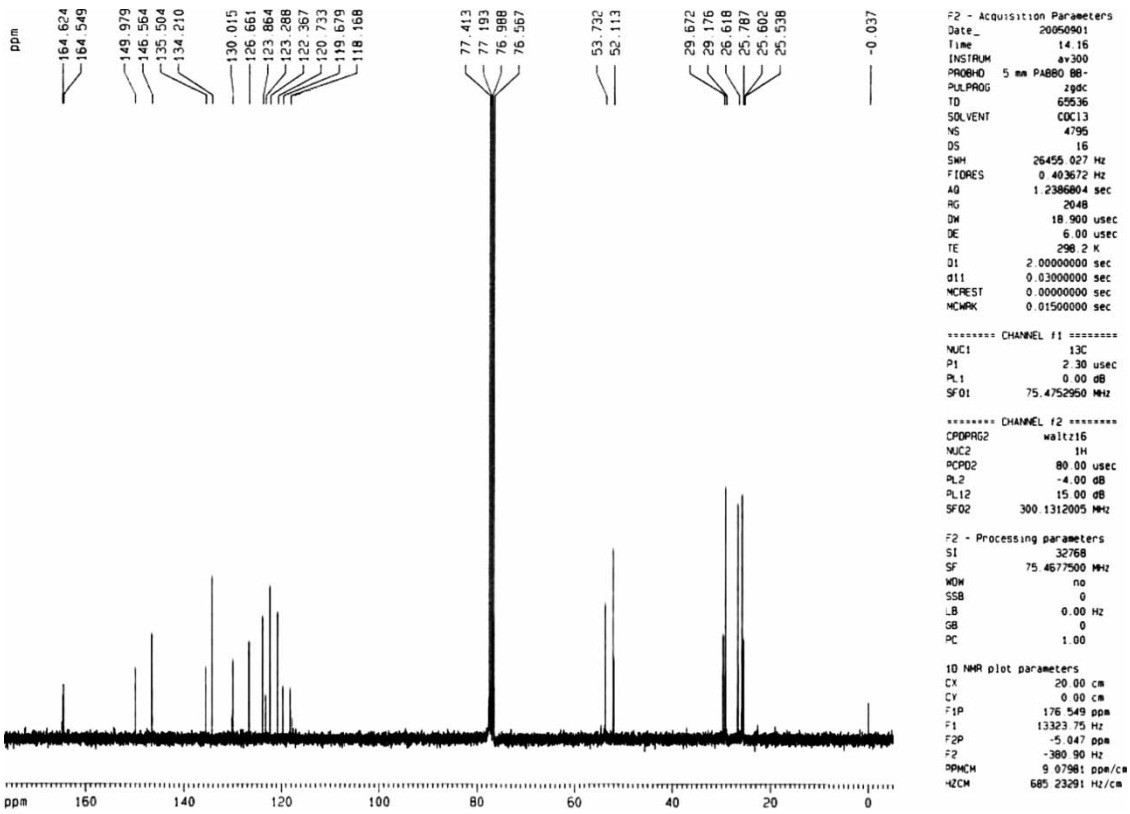

FIGURE A4 ^{13}C-NMR spectrum of compound **4**b.